Monitoring water vapour with GNSS during a heavy rainfall event in the Spanish Mediterranean area

E. Priego, J. Jones, M.J. Porres & A. Seco

Taylor & Francis
Taylor & Francis Group

Monitoring water vapour with GNSS during a heavy rainfall event in the Spanish Mediterranean area

E. Priego [ID][a], J. Jones[b], M.J. Porres [ID][a] and A. Seco[c]

[a]Universitat Politècnica de Valencia, Camino de Vera, Valencia, Spain; [b]Met Office, Fitzroy Road, Exeter, United Kingdom; [c]Public University of Navarre, Campus de Arrosadia, Pamplona, Spain

ABSTRACT

The Spanish Mediterranean area is periodically affected by torrential rainfall events during autumn. In September 2012, one of these episodes took place with up to 50 mm of rain in a 1-hour period and with more than 300 mm in 12 hours. This study shows the spatial and temporal variability of the atmospheric integrated water vapour (IWV) observed using delays in Global Navigation Satellite System (GNSS) signals and associated rainfall during this severe weather event. This experiment focuses on the relationship between the variations of IWV values in GNSS stations and meteorological variables such as atmospheric pressure and precipitation. This study was carried out on the Mediterranean coast of Spain during a heavy rainfall episode. The results show a mean increase in IWV of around 30 kg/m^2 occurring prior to heavy precipitation. They further revealed an increase of up to a 100% in IWV values in several GNSS stations available in the study area. Fluctuations in IWV fields correlate well with approaching frontal rainfall and a combined rise in IWV and a drop in atmospheric pressure may well be used as a pre-cursor to heavy precipitation.

1. Introduction

Heavy rainfall is generally associated with high moisture content, vertical movement and static instability (Maddox 1979; Doswell et al. 1996). Forecasting precipitation in the Western Mediterranean is difficult because of the interactions between dynamical forcing, orographic lifting and moisture advection from the warm Mediterranean Sea (Vedel et al. 2004). One of the main characteristics that define rainfall in this region is the variability in the volume of the precipitation, an interesting aspect however is the extraordinary rainfall intensity shown in some episodes. Predicting the development of severe weather phenomena such as storm evolution is highly dependent on very precise estimates of water vapour contained within the lower atmosphere (Choy et al. 2013). Atmospheric water vapour content also occurs in this region with greater variability and instability, which is intrinsically linked to heavy rainfall.

This type of event motivated an effort to improve precipitation forecasting by incorporating additional information on the initial state of the humidity field from Global Navigation Satellite System (GNSS) observations (Vedel et al. 2004). The non-hydrostatic component of GNSS signal delays is largely attributable to the amount of atmospheric water vapour. So, thanks to the permanent GNSS stations worldwide, atmospheric water vapour can be continuously estimated, thus improving forecast skill in distribution of humidity fields.

CONTACT E. Priego ✉ epriego@cgf.upv.es

GNSS technology has long since demonstrated its capacity as an accurate sensor of atmospheric water vapour with the application of GNSS for numerical weather prediction (NWP). However, the potential of GNSS tropospheric delays for forecasting very short-term severe weather, in particular for monitoring intense precipitation and its association with convection, has only more recently been demonstrated (Graham et al. 2012; Seco et al. 2012; de Haan 2013).

This case study shows an experimental analysis concerning the spatial and temporal variability of integrated water vapour (IWV) during a heavy rainfall episode. This episode occurred in autumn 2012, which affected several regions of Spain, causing large economic losses and loss of life.

The synoptic situation associated with the heavy rainfall was dominated by a low pressure system located in the western/south-western Iberian Peninsula with advection of warm, moist air at low levels from the south or South-west from the Mediterranean Sea. The sea surface temperature was 23 °C, with air temperature of 14 °C at the 850 hPa pressure level. Figure 1 shows the centre of the low pressure system located over North Africa, a low pressure over the eastern Mediterranean Sea and an anti-cyclonic over much of western to central Europe (27 September 2012 at 00 hours UTC).

2. Data and methods

2.1. GNSS data

GNSS IWV estimates were obtained from 38 sites available from the Spanish Mediterranean Area (Figure 2) courtesy of the National Geographical Institute (IGN), the CATNET network of the Cataluña Cartographic Institute (ICC), the ERVA network of the Valencia Cartographic Institute (ICV), the Meristemum network of the Region of Murcia (REGAM), and from the RAP network in Andalucia (Table 1). Data was collected for the period between 24 and 30 September 2012 (i.e. a one-week period, a few days prior to, and after the severe weather event).

2.2. Meteorological data

All meteorological data (atmospheric pressure and precipitation observations) were supplied by the Spanish Meteorology Agency (AEMET). The meteorological observing stations are distributed throughout the study area and collocated with the GNSS stations with precipitation observations available with a 1-hour frequency.

In addition, three GNSS sites situated very close to three radiosonde stations (Vaisala RS92SGP) were used to verify the GNSS IWV estimates. Radiosonde integrated precipitable water vapour (RS-IWV) observations have a 12-h interval with observations at 00:00 hours UTC and 12:00 hours UTC. Radiosonde data were available for the period 2006−2011 at Zaragoza and Murcia, and 2001−2011 at Mallorca (Table 2).

2.3. Theory and calculation

The effect of the troposphere causes delays in GNSS signal propagation which can be expressed in a first approximation as the integral of the atmospheric refractivity (N), along the signal path (ds):

$$Ls = \int (n-1)ds = 10^{-6} \int N(s)ds. \tag{1}$$

27SEP2009 12Z
500 hPa Geopotential (gpdm) und Bodendruck (hPa)

28SEP2009 12Z
500 hPa Geopotential (gpdm) und Bodendruck (hPa)

29SEP2009 12Z
500 hPa Geopotential (gpdm) und Bodendruck (hPa)

Daten: Reanalysis des NCEP
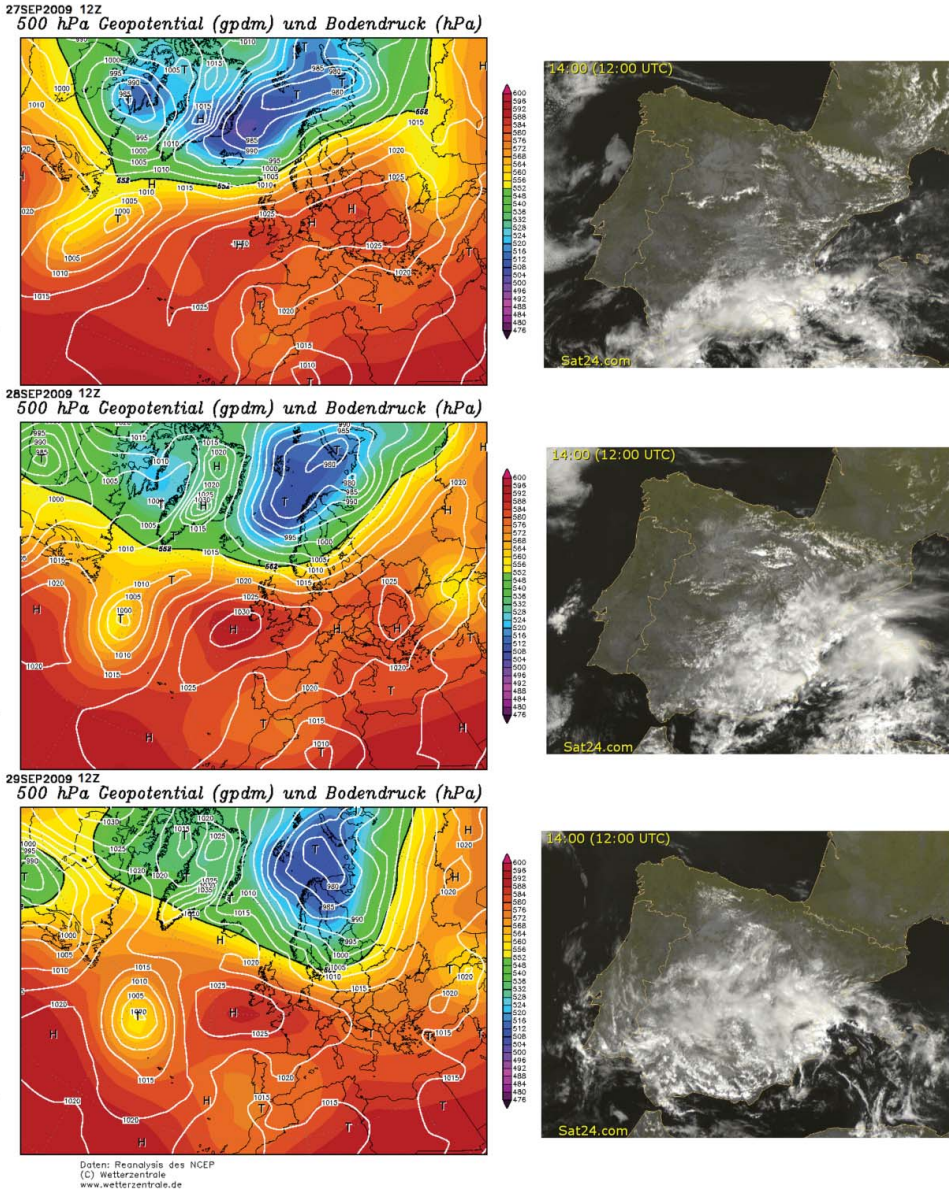(C) Wetterzentrale
www.wetterzentrale.de

Figure 1. 500-hPa geopotential height observed on 27, 28 and 29 September 2012 at 12:00 hours UTC (Wetterzentrale). Cloud satellite images taken on 27, 28 and 29 September 2012 at 12:00 hours UTC (Sat24).

Refractivity (N) can be described as a function of meteorological parameters from the empirical expression (Essen and Froome 1951; Hartmann and Leitinger 1984):

$$N = K_1 \frac{P}{T} + K_2 \frac{e}{T} + K_3 \frac{e}{T^2}, \tag{2}$$

where K_1, K_2 and K_3 are empirically determined coefficients, P is the surface atmospheric pressure (hPa), e is the water vapour pressure (hPa) and T is the temperature (K).

Figure 2. Study area in Spain (black area) and GNSS and radiosounding station locations. To view this figure in colour, see the online version of the journal.

Table 1. GNSS stations coordinates.

GNSS station ID	GNSS station (full name)	Longitude	Latitude	Altitude	Organization
ALAC	Alicante	−0°28′52″	38°20′20″	60,36	IGN
ALBA	Albacete	−1°51′23″	38°58′40″	751,74	IGN
ALME	Almería	−2°27′34″	36°51′09″	127,52	IGN
BCLN	Barcelona	2°00′15″	41°24′19″	84,82	IGN
CEU1	Ceuta	−5°18′23″	35°53′31″	52,47	IGN
COBA	Córdoba	−4°43′16″	37°54′56″	202,08	IGN
GIRO	Girona	2°51′18″	42°02′29″	112,72	IGN
HUEL	Huelva	−6°55′13″	37°11′59″	81,86	IGN
MALA	Málaga	−4°23′36″	36°43′34″	119,85	IGN
MALL	Mallorca	2°37′28″	39°33′09″	62,06	IGN
TARI	Tarifa	−5°36′09″	36°00′30″	49,94	IGN
TERU	Teruel	−1°07′27″	40°21′01″	956,19	IGN
ZARA	Zaragoza	−0°52′55″	41°38′00″	296,11	IGN
BELL	Bellmunt	1°24′04″	41°35′58″	853,42	ICC
EBRE	Ebro (obs)	0°29′32″	40°49′15″	107,81	ICC
LLEI	Lleida	0°35′46″	41°37′45″	254,34	ICC
ESCO	Escornacrabes	0°58′32″	42°41′36″	2508,00	ICC
REUS	Reus	1°10′06″	41°10′12″	173,44	ICC
ALCO	Alcoy	−0°28′24″	38°41′52″	640,09	ICV
AYOR	Ayora	−1°12′30″	39°03′40″	661,82	ICV
BERG	Bergantes	−0°05′50″	40°36′41″	892,80	ICV
BORR	Burriana	−0°04′59″	39°54′18″	72,90	ICV
DENI	Denia	0°06′13″	38°50′05″	69,67	ICV
TORR	Torrevieja	−0°40′51″	37°58′31″	57,11	ICV
UTIE	Utiel	−1°12′30″	39°34′07″	799,70	ICV
VCIA	Valencia	−0°20′38″	39°26′08″	62,95	ICV
CRVC	Crevillente	−1°52′07″	38°06′52″	738,78	REGAM
CRTG	Cartagena	−0°59′43″	37°36′22″	65,34	REGAM
JUMI	Jumilla	−1°19′37″	38°28′16″	553,12	REGAM
LORC	Lorca	−1°41′12″	37°39′14″	365,72	REGAM
MURC	Murcia	−1°07′28″	37°59′31″	125,15	REGAM
UCAD	U. Cádiz	−6°12′37″	36°43′34″	65,30	RAP
GRA1	Granada	−3°35′47″	37°11′23″	823,27	RAP
HUOV	Huércal-Overa	−1°56′31″	37°24′05″	352,21	RAP
UJAE	U. Jaen	−3°46′54″	37°47′15″	527,77	RAP
MOTR	Motril	−3°31′13″	36°45′17″	166,97	RAP
SEVI	Sevilla	−5°58′17″	37°20′44″	102,96	RAP
ROND	Ronda	−5°08′36″	36°45′14″	809,62	RAP

Table 2. Radiosounding stations coordinates. Horizontal and vertical differences between radiosounding stations and GNSS stations. IWV-radiosonde and IWV-GNSS comparison.

Radiosounding station	Longit.	Latitude	Altitude (m)	Horizontal difference (km)	Vertical difference (m)	Number of pairs	Std. Dev. (mm)	RMS (mm)	GNSS station
08160 — Zaragoza	−1°01′	41°39′	258	11	38	2607	2.84	2.84	ZARA — Zaragoza
08302 — Mallorca	2°37′	39°33′	62	10	21	5102	2.77	1.47	MALL — Mallorca
08430 — Murcia	−1°17′	38°00′	62	14	13	2625	2.94	3.34	MURC — Murcia

The zenith total delay (ZTD) is the sum of the two components:

$$ZTD = ZHD + ZWD, \tag{3}$$

The hydrostatic component caused by the atmospheric dry gases and aerosols, zenith hydrostatic delay (ZHD) and the second component is primarily due to atmospheric water vapour and is known as zenith wet welay (ZWD).

ZHD contributes to more than 90% of the ZTD and it is relatively stable. ZHD is directly proportional to atmospheric pressure and it can be determined with an accuracy that is better than 1% using the Saastamoinen model. ZHD can be estimated from the following expression (Saastamoinen 1972):

$$ZHD = \frac{k_1 * R_d * P_a}{9.784\left(1 - 0.0026 * \cos(2\phi) - 2.8 * 10^{-7} * H_a\right)} * 10^{-3} \, (mm), \tag{4}$$

where K_1 is the refractivity constant = 77.60 K/hPa ± 0.05 K/hPa (Bevis et al. 1994), R_d is the specific gas constant of dry air (287.058 J kg^{-1} K^{-1}), φ is the latitude in degrees and H_a is the surface height above the ellipsoid in km.

ZWD is responsible for most of the short-term variation in ZTD due of the heterogeneity of the water vapour content in the atmosphere. As such modelling of this property is not possible (Haase et al. 2003) and must be estimated using GNSS processing software.

In this study, ZTD values were processed using the GAMIT GNSS processing software. The values of ZTD were set as a stochastic variation of the Saastamoinen model with piecewise linear interpolation of the data within the processing epoch (Herring et al. 2006). The first calculation provides precise coordinates for the local stations for each 24 hours of measurements, where tropospheric parameters have been estimated with a 2 hourly resolution (Brenot et al. 2006). The final positions of the stations in the ITRF2000 reference frame (Altamimi et al. 2002) were obtained in a global solution using the Kalman filter. Subsequent zenith delays are calculated hourly. Baselines greater than 2000 km have been used in order to decorrelate the tropospheric parameters from vertical position estimations (Tregoning et al. 1998). The Global Mapping Function (GMF) was used to map the slants to the zenith (Boehm et al. 2006) and the raw RINEX format data were used with a sampling rate of 30 seconds and an elevation cut-off angle of 10° (Pacione et al. 2001).

ZTD measurements have been produced using a sliding window strategy, with sessions of 25 hours shifted by 12 hours. The system uses two 25-hour sliding windows for each day to obtain hourly ZTD values, removing the first six and last seven values from each sliding window. The system uses only 12 central values from each window to avoid the edge effect of the Gauss-Markov process (Jin et al. 2007).

Furthermore, if the mean atmospheric temperature (T_m) is calculated, ZWD can be easily converted to IWV, according to Bevis et al. (1994):

$$IWV = \frac{10^{-6}}{R_w \cdot \left(k_2' + \frac{k_3}{T_m} \right)} \cdot ZWD, \tag{5}$$

where R_W is the specific gas constant of water vapour (461.495 J kg^{-1} K^{-1}), $k_2' = 70.4 \pm 2.2$ K/hPa (Bevis et al. 1994), $k_3 = 3.739 \pm 0.012 \ 10^5$ K/hPa (Bevis et al. 1994) and T_m is the weighted mean atmospheric temperature.

3. Results and discussion

3.1. GNSS-IWV and RS-IWV analysis

The radiosonde profiles provide atmosphere information up to an altitude of approximately 30 km. The radiosonde balloons are released every 12 hours in most cases. The radiosonde IWV is taken as another independent reference data for validation of the GNSS-IWV (Xingxing et al. 2015). To perform a processing strategy verification check, three radiosonde time-series data (RS-IWV) were compared against GNSS data (GNSS-IWV) estimates at ZARA-Zaragoza (ZARA) and Murcia (MURC) for a period of 6 years between 2006 and 2011, and for the station in Mallorca (MALL), for a period of 11 years between 2001 and 2011. Table 2 shows the approximate position of the radiosonde stations and horizontal and vertical distances between radiosonde and GNSS stations. It further shows the total number of pairs, the standard deviation and the root mean square (RMS). The RMS values of the IWV differences are 2.84 mm for Zaragoza, 3.34 mm for Murcia and 1.47 mm for Mallorca.

Figure 3 shows the correlation between the values GNSS-IWV and RS-IWV, where $R^2 = 0.87$ and PCC (Pearson correlation coefficient) $= 0.93$ for Zaragoza; $R^2 = 0.89$ and PCC $= 0.94$ for Murcia; and $R^2 = 0.89$ and PCC $= 0.95$ for Mallorca were obtained.

These results demonstrate the quality of the GPS processing strategy and the capability of the GNSS to accurately measure atmospheric water vapour content.

Figure 4 shows the evolution of IWV for one month (July 2012) with both techniques, for each of the three stations. From a spatial and temporal point of view, GNSS technology offers substantially more information in regards to the content of atmospheric water vapour than is available from radiosounding.

3.2. Case study

3.2.1. Time evolution IWV-pressure-precipitation

During the events of the 27−29 of September 2012, heavy rainfall occurred when there was an increase of IWV and a relatively sharp fall of the atmospheric pressure. Figure 5(a) shows the spatial distribution of IWV along the Spanish Mediterranean coast on a specific day and time (28 September at 14:00 hours UTC). It can be seen as the highest values was recorded in the area of Murcia (IWV = 44 mm) and Valencia (IWV = 39 mm).

The solutions obtained in this analysis for each of the 38 GNSS reference stations used in this study suggest that heavy rainfall events in this region are correlated with a decrease in atmospheric pressure and a simultaneous increase of atmospheric IWV content. Figure 5(b) shows time evolution of IWV in mm (green line) and atmospheric pressure in hPa (red line) along with rainfall amount (blue bar) registered during the period of study (from 24 to 30 September) at different stations along the study area. The accumulated rainfall data are hourly values (mm).
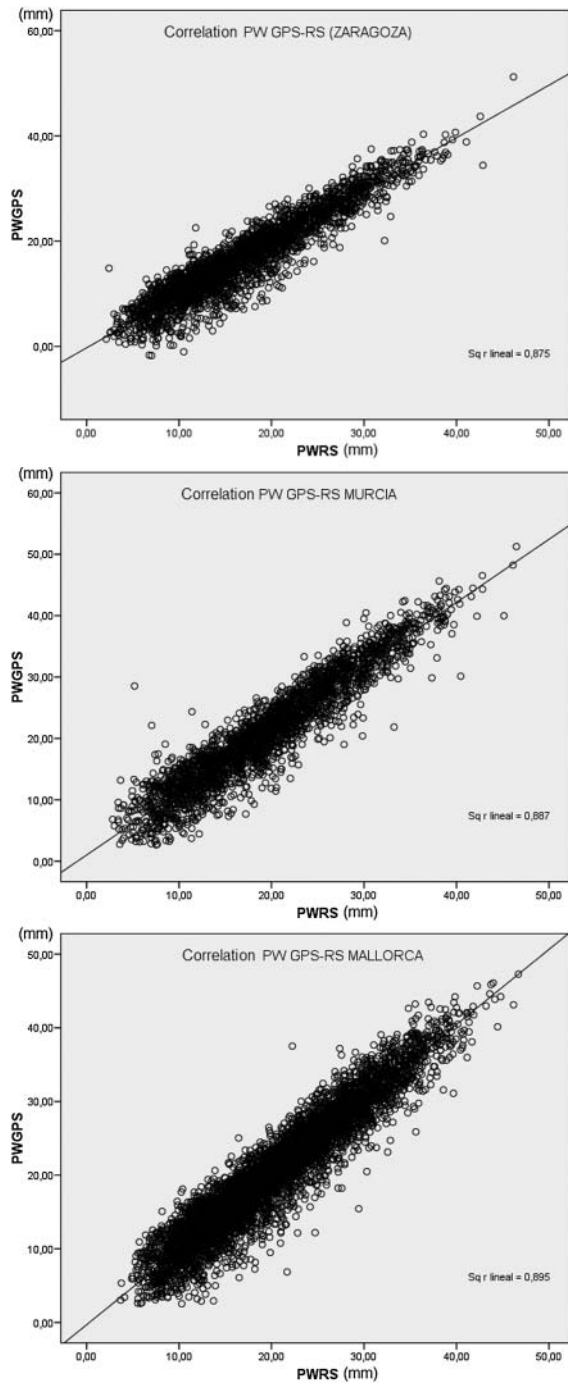
Figure 3. Comparison of radiosounding system and GNSS IWV values (Zaragoza − ZARA, Murcia − MURC and Mallorca − MURC).

Rainfall values reached 50 mm on average for all precipitation stations; Valencia recorded 198 mm of rain throughout the study period (112 mm in Cadiz, 82 mm in Reus, 75 mm in Murcia and 64 mm in Motril). In addition, the highest amount of precipitation recorded in Valencia within 1 hour was 68 mm (23 mm in Cadiz, 27 mm in Reus, 36 mm in Murcia and 31 mm in Motril).
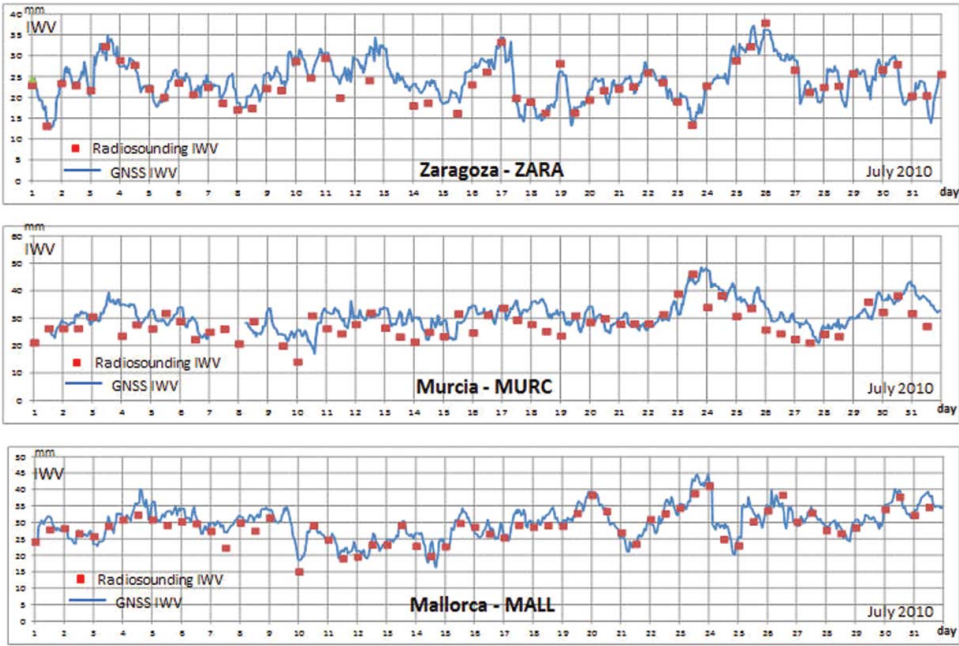
Figure 4. GNSS-IWV and radiosounding-IWV analysis (July 2010).
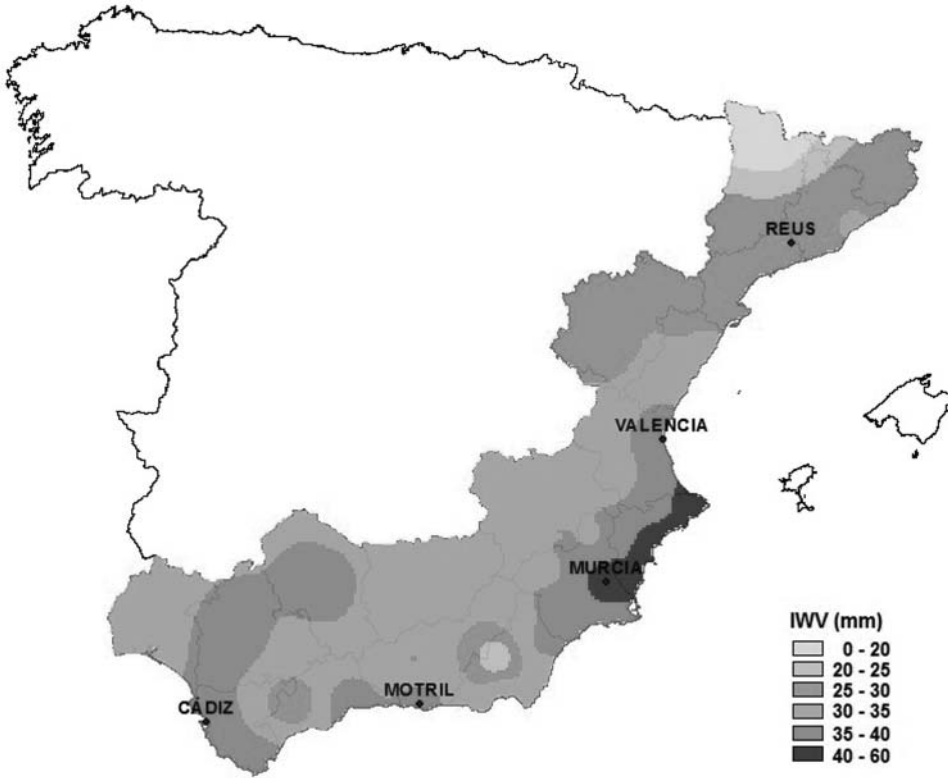

Figure 5. (a) Spatial distribution of IWV along the Spanish Mediterranean coast (28 September 2012 at 14:00 hours UTC) and locating stations. (b) Time evolution of IWV and atmospheric pressure along with the amount of rainfall registered during the period from 24 to 30 September 2012 at different stations along the study area. To view this figure in colour, see the online version of the journal.
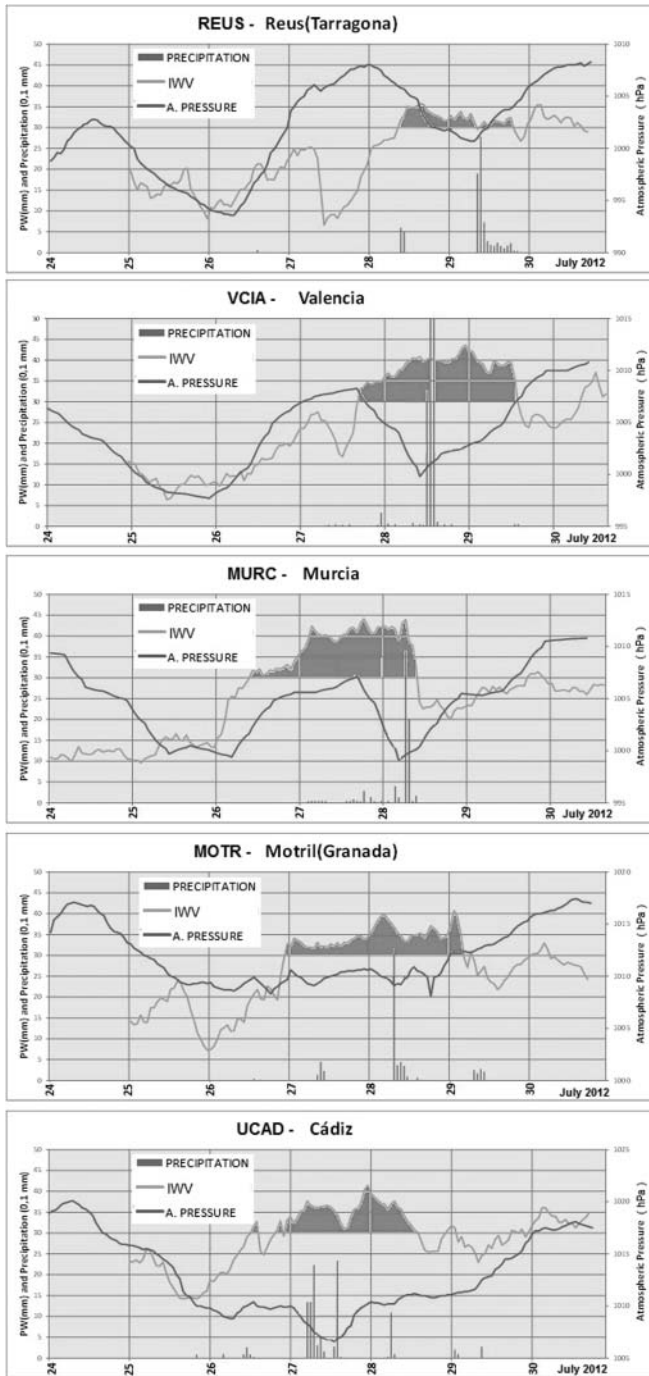
Figure 5. (*Continued*)

For all examples, there is a large decrease in atmospheric pressure (mean decrease in pressure of 10 hPa for the 38 stations used in the study), in a relatively short period of time. The fall in atmospheric pressure occurs up to 24 hours prior to the rainfall, but in the majority of cases, the drop in atmospheric pressure occurs around 12 hours prior to precipitation, with pressure decreasing from 5 to 15 hPa in a 12-hour period. This is particularly pronounced in Murcia and Valencia.

The IWV trend provides additional information with a mean increase in IWV of around 30 kg/m^2 occurring prior to the heavy precipitation event. This indicator operates in the same way for all stations in this study. The area below the IWV line and above 30 kg/m^2 is the graphical threshold in each case and is shaded green. In this study we have used the absolute values of IWV, without considering the altitude correction of the stations.

Changes in IWV followed by a sharp decrease in atmospheric pressure do seem to correlate with heavy precipitation. In the majority of cases, IWV greatly increased between 24 and 48 hours prior to the most intense rainfall, and then with a sharp decrease at or soon after the rainfall event indicating there was no more atmospheric water vapour available to precipitate out as rain. In this case study, the large increase and decrease of atmospheric water vapour does seem to define the beginning and the end of the severe weather event.

3.2.2. IWV monitoring

Two-dimensional (2D) IWV maps have been developed using the inverse distance weighting (IDW) interpolation method to show the spatial variability of IWV. This method converts point data into a continuous surface, allowing the spatial and temporal behaviour of IWV and rainfall to be analyzed (Figures 6 and 7). Figure 6 is a series of IWV maps illustrating the evolution of IWV in the region over the period of the case study (2-h temporal resolution from 28 September at 08:00 hours UTC to 29 September at 08:00 hours UTC).

It can be seen that within a few hours, there is an increase in IWV in the south of the Iberian Peninsula. There is also the eastern Spain area, where the values of IWV are consistently high throughout the period of study. (NB: Previous days' IWV maps illustrate a general stability and homogeneity in the region, with IWV values typically lower than 20 mm.) IWV values begin to increase quickly primarily in the south and southwest, correlating well with the region of heavy precipitation. By 30th of September, it can be seen that the IWV has decreased significantly to pre-event levels, thus signifying the end of the severe weather event.

Figure 7 illustrates an hourly accumulated precipitation map, clearly showing areas where intense precipitation has occurred (dark shading). As the storm moves to the east, two episodes of major rainfall occur. The first occurs during the morning of 28th September with rainfall at Lorca (LORC) exceeding 140 litres in a 6-hour period (and a peak of more than 50 litres per hour recorded). Also at Almeria (ALME) an accumulated value of 315 litres in 7 hours was recorded (with peak values of more than 70 litres per hour recorded at 10:00 hours UTC). In this case, the values of IWV increased considerably between 3 and 6 hours prior to the arrival of the rain.

The second episode is focused on the region of Valencia (VCIA), in which intense rainfall occurred during the afternoon of 28 September 2012. In one case, 40 litres per hour was recorded in Alicante (ALAC), and an accumulated value of 184 litres was recorded near the city of Valencia, where 24 hours earlier the IWV suffered an increase of more than 20 mm.

Finally, one last front affected the Cataluña region (REUS, BCNA) due to another storm front coming in from the Mediterranean Sea which affected the northeast of the Iberian Peninsula, producing rainfall values of up to 28 mm per hour.

4. Conclusions

In this paper, the relationship between heavy rainfall and water vapour content have been analyzed in an area prone to some of the highest values of IWV in Europe. IWV values are higher in the central area of the study zone. In this area, the contribution of moisture from the Mediterranean Sea
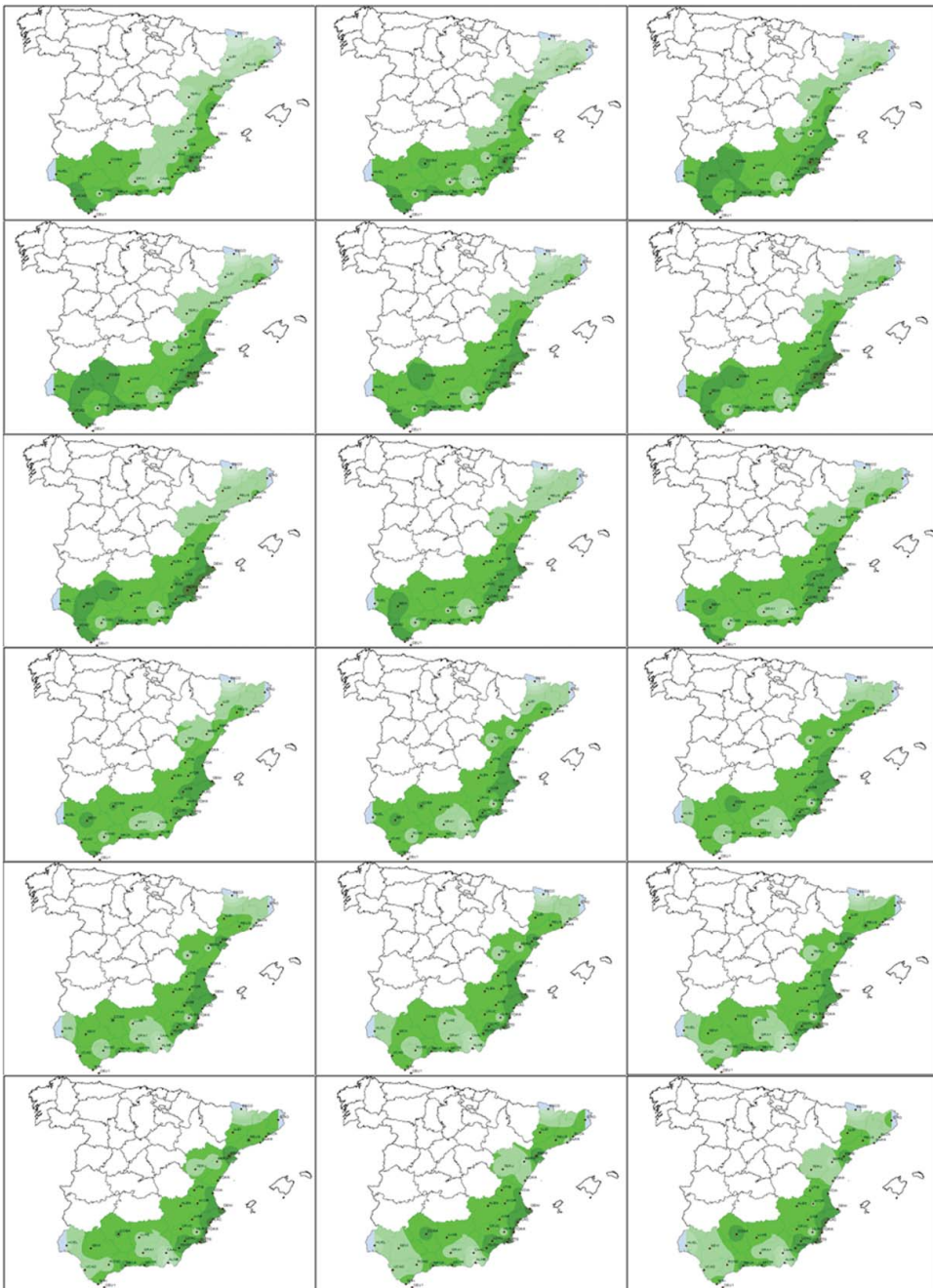
Figure 6. IWV map 24 hours monitoring in 2 h (from 28th September 8:00 am until 29th September 8:00 am).

and the structured topographic relief contributes to moist air flows, allowing a continuous feed of atmospheric water vapour.

The results presented here indicate an apparent link between when pressures drop and when there are high levels of IWV, severe precipitation events occur. All GNSS stations show a quick and clear increase in IWV a few hours before the onset of precipitation. In addition, the maximum value of IWV occurs almost simultaneously with the peak intensity of rain.
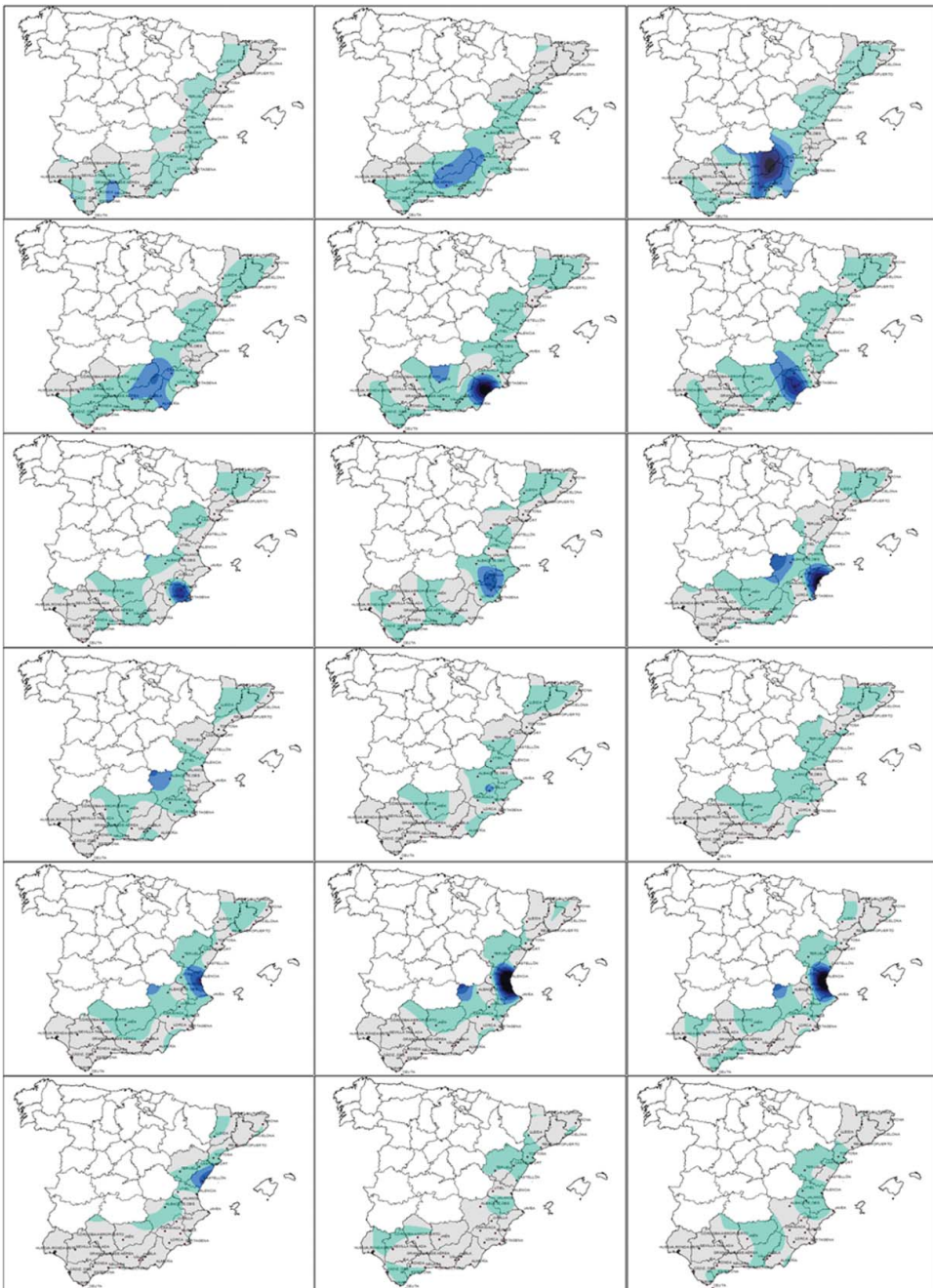
Figure 7. Rainfall monitored for 24 hours in 2-h bins (from 28th September 8:00 hours UTC to 29th September 8:00 hours UTC).

However, new studies should be established in the future to quantify this apparent relationship and it could be the basis for the implementation of a severe weather warning system. A setting for three parameters will be used. The first parameter would be the time-window before and after the highest rain accumulation of an event. The second parameter would be the rise of IWV during the time window, and the third parameter the rise or fall of pressure.

GNSS are an effective tool for atmospheric monitoring, which allow us to improve the spatial and temporal determination of the atmospheric water vapour content.

Disclosure statement

No potential conflict of interest was reported by the authors.

ORCID

E. Priego 🅙 http://orcid.org/0000-0001-6642-7806
M.J. Porres 🅙 http://orcid.org/0000-0002-7913-4436

References

Altamimi Z, Sillard P, Boucher C. 2002. ITRF 2000: a new reléase of the international terrestrial reference frame for earth science applications. J Geophys Res. 107:2214.

Bevis M, Businger S, Chiswell S, Herring TA, Anthes R, Rocken C, Ware R. 1994. GPS Meteorology: mapping zenith wet delays onto precipitable water. J Appl Meteorol. 33:379−386.

Boehm J, Niell A, Tregoning P, Schuch H, 2006. Global Mapping Function (GMF): a new empirical mapping function based on numerical weather model data. Geophys Res Lett. 33:L07304.

Brenot H, Ducrocq V, Walpersdorf A, Champollion C, Caumont O. 2006. GPS zenith delay sensitivity evaluated from high-resolution numerical weather prediction simulations of the 8e9 September 2002 flash flood over southeastern France. J Geophys Res. 111:D15105.

Choy S, Wang C, Zhang K, Kuleshov Y. 2013. GPS sensing of precipitable water vapour during the March 2010 Melbourne storm. Adv Space Res. 52:1688−1699.

de Haan S. 2013. Assimilation of GNSS ZTD and radar velocity for the benefit of very-short-range regional weather forecast. Q J R Meteorolog Soc. 677:2097−2107.

Doswell CA, Brooks HA, Maddox RA. 1996. Flash flood forecasting: an ingredients-based methodology. Weather Forecasting. 22:981−1002.

Essen L, Froome KD. 1951. The refractive indices and dielectric constants of air and its principal constituents at 24 GHz. Proc Phys Soc. 64:862−875.

Graham E, Koffi EN, Maetzler C, 2012. An observational study of air and water vapour convergence over the Bernese Alps, Switzerland, during summertime and the development of isolated thunderstorms. Meteorol Z. 21:561−574.

Haase J, Ge M, Vedel H, Calais E. 2003. Accuracy and variability of GPS tropospheric delay measurements of water vapour in the Western Mediterranean. J Appl Meteorol. 42:1547−1568.

Hartmann GK, Leitinger R. 1984. Range errors due to ionospheric and tropospheric effects for signal frequencies above 100 MHz. B Géod. 58:109−136.

Herring T, King R, McClusky S. 2006. GAMIT reference manual. Department of Earth, Atmospheric, and Planetary Sciences.

Jin S, Park JU, Cho JH, Park PH. 2007. Seasonal variability of GPS-derived zenith tropospheric delay and climate implications. J Geophys Res. 112:D09110.

Maddox RA. 1979. A methodology for forecasting heavy convective precipitation and flash flooding. Natl Weather Dig. 4:30−42.

Pacione R, Sciarretta C, Vespe F, Faccani C, Ferretti R, Fionda E, Ferraro C, Nardi A. 2001. GPS meteorology: validation and comparisons with ground-based microwave radiometer and mesoscale model for the Italian GPS Permanent Stations. Phys Chem Earth. 26:139−145.

Saastamoinen J. 1972. Atmospheric correction for the troposphere and stratosphere in radio ranging of satellites. The Use of Artificial Satellites for Geodesy, Geophysics Monograph Series, American Geophysics. 15:245−251.

Seco A, Ramírez F, Serna E, Prieto E, García R, Moreno A, Cantera JC, Miqueleiz L, Priego E. 2012. Rain pattern analysis and forecast model based on GPS estimated atmospheric water vapour content. Atmos Environ. 49:85−93.

Tregoning P, Boers R, O'Brien D, Hendy M. 1998. Accuracy of absolute precipitable water vapor estimates from GPS observations. J Geophys Res. 103:701−710.

Vedel H, Huang XY, Haase J, Ge M, Calais E. 2004. Impact of GPS ZTD data on precipitation forecast in Mediterranean France and Spain. Geophysical Research Letters. 31:L02102.

Xingxing L, Dick G, Cuixian L, Maorong G, Nilsson T, Ning T, Wickert J, Schuh H. 2015. Multi-GNSS meteorology: real-time retrieving of atmospheric water vapour from BeiDou, Galileo, GLONASS and GPS observations. IEEE Trans Geosci Remote Sens. 53:6385−6393.